Liquid Crystals, Vol. 32, No. 8, August 2005, 985–995

Taylor & Francis
Taylor & Francis Group

A comparison of mesogenic properties of *p*-carborane-1,12-dicarbaldehyde schiff's bases with their terephthaldehyde analogues

TAKASHI NAGAMINE†, ADAM JANUSZKO‡, KIMINORI OHTA†, PIOTR KASZYNSKI*‡ and YASUYUKI ENDO†

†Tohoku Pharmaceutical University, 4-4-1, Komatsushima, Aoba-ku, Sendai 981-8558, Japan
‡Organic Materials Research Group, Department of Chemistry, Vanderbilt University, Nashville, TN 37235, USA

(*Received 8 March 2005; in final form 28 June 2005; accepted 2 July 2005*)

A homologous series of carborane-containing Schiff's bases **1A[*n*]** (n=1–10) was prepared and compared with the analogous series **1B[*n*]** derived from terephthaldehyde. An exponential fit of the T_{NI} values for both series yielded a quantitative assessment of the effect of ring structure on mesophase stability. This includes the T_{NI} value for $n\rightarrow\infty$ (86°C for **1A[*n*]** and 209°C for **1B[*n*]**) and steepness of descent (0.135 for **1A[*n*]** and 0.095 for **1B[*n*]**). The difference in behaviour of the two series was attributed, largely, to conformational properties of the central rings **A** and **B**. Electronic interactions between the central rings and the π-substituents were investigated by UV spectroscopy and by quantum-mechanical calculations. The effect of replacement of O with CH_2 in the terminal chain of **1[*n*]** on the namatic phase stability was assessed for n=5–7.

1. Introduction

Our previous comparative studies indicate that a carborane cluster (figure 1) incorporated into a mesogenic molecule strongly destabilizes smectic phases and generally lowers the clearing temperatures when compared with the isostructural mesogenic derivatives of benzene, bicyclo[2.2.2]octane, and cyclohexane [1–5]. Recently, we began investigations of homologous series of mesogenic derivatives of carboranes and compared the observed trends with those found in the series of hydrocarbon analogues. In this context, we have investigated a series of diesters [6] containing two alkyl chains up to n-$C_{22}H_{45}$ and a less extensive series of dioxanes [7]. We found exclusively nematic behaviour and exponential descent of the T_{NI} values in both series with increasing chain length.

Here, we report a homologous series of Schiff's bases **1A[*n*]** with n=1–10 and detailed comparison of their mesogenic behaviour with that found in the benzene analogues **1B[*n*]**. We have also investigated the effect of replacement of the linking oxygen atom with the CH_2 group in three carborane analogues **2A[*n*]**. In order to explain the observed differences between series **1A[*n*]** and **1B[*n*]**, we have investigated conformational and electronic properties of carborane and benzene Schiff's bases. In this context, we discus UV-vis spectra for a representative member of each series.

*Corresponding author.
Email: piotr.kaszynski@vanderbilt.edu

2. Results and Discussion

2.1. *Synthesis*

Schiff's bases **1[*n*]** and **2A[*n*]** were prepared by acid-catalysed condensation of the appropriate dialdehyde **3** and substituted aniline (scheme 1). *p*-Carborane-1, 12-dicarbaldehyde (**3A**) was conveniently prepared by Dess–Martin oxidation [8] of *p*-carborane-1,12-dimethanol (**4A**, scheme 2). The diol was obtained from *p*-carborane according to a modified literature procedure [9].

2.2. *Mesogenic properties*

Phase transition temperatures and enthalpies for the investigated compounds are collected in tables 1 and 2.

A **B**

Figure 1. *p*-Carborane (**A**) and benzene (**B**). In **A** each vertex corresponds to a BH fragment and the sphere represents a carbon atom.

Liquid Crystals
ISSN 0267-8292 print/ISSN 1366-5855 online © 2005 Taylor & Francis
http://www.tandf.co.uk/journals
DOI: 10.1080/02678290500291756

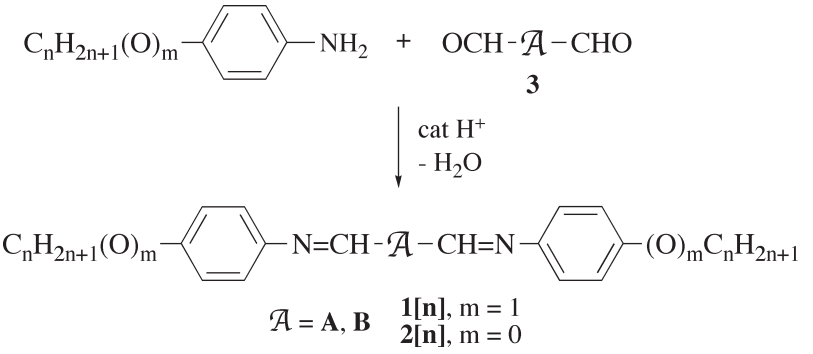

Scheme 1.

Phase structures were assigned by comparison of microscopic textures observed in polarized light with those published for reference compounds [10, 11].

All the carborane derivatives **1A[*n*]** (n=1–10) show only nematic behaviour. Most of the compounds exhibit monotropic nematic phases, while **1A[1]** and **1A[4]** form narrow range, <10°C wide enantiotropic phases. The clearing temperatures in the series decrease with increasing length of the alkyl chain and exhibit the typical 'odd–even' effect (figure 2).

A comparison of the carborane series **1A[*n*]** with the benzene homologous series **1B[*n*]** [12–15] reveals significant differences. The nematic-isotropic transition temperatures T_{NI} for the carborane Schiff's bases are lower by an average of 137°C (±6°C) than for the benzene analogues. Also, the onset of smectic behaviour is observed for early homologues of the benzene series (**1B[4]**) [12], while no smectic phase was found even in **1A[10]**, the longest carborane homologue presently investigated (table 1). This highly nematogenic behaviour of the carborane series is consistent with our findings for an analogous series of diesters which exhibits purely nematic properties [6].

Numerical analysis revealed an exponential decay of the T_{NI} values with increasing chain length in both series (figure 2), and the data was fitted to a four-parameter function [6, 16], Equation (1).

$$T_{NI} = a + \exp\left(b - c \times n^{d}\right). \quad (1)$$

The limiting values a $\left[\lim_{n\to\infty} T_{NI}(n) = a\right]$ obtained for both odd and even n series of **1A[*n*]** were 85.3±1.1 and 86.6±3.6°C with the overall high correlation factor $\mathcal{R}^2$ of 1 and 0.9999 for each fit, respectively. This consistency of the T_{NI} for infinite n and the quality of correlation in both fittings reflects the high degree of internal consistency of the measurements and high purity of the compounds. For further analysis, the limit a in **1A[*n*]** was fixed at 86°C without significant change in $\mathcal{R}^2$. Similar analysis for the benzene analogues **1B[*n*]** revealed satisfactory (albeit lower quality), correlations only for the odd n series (a=209±8°C, $\mathcal{R}^2$), while poor correlation and large errors were obtained for the series with even n (a=207±52°C, $\mathcal{R}^2$=0.996). The former series was investigated in our laboratory and the lower quality of correlation is largely due to the uncertainty of the high temperature data for **1B[1]** and **1B[3]**, which partially decompose or sublime at the T_{NI}. The relatively large errors observed for the even n series demonstrates internal inconsistency between our data for **1B[2]** and **1B[10]** and three datapoints taken from the literature, in addition to problems with high T_{NI} for **1B[2]**. Thus, the limit a in **1B[*n*]** was set for 209°C, and further analysis relies on parameters obtained for the odd n series.

The exponential parameter d in equation (1) appears to be characteristic for the general type of mesogenic derivatives. The close values for **1A[*n*]** (1.397 and 1.381) and **1B[*n*]** (1.320) were averaged to 1.35 and this value was used for subsequent analysis of both series. Further analysis revealed close values for the pre-exponential factor c (−0.1375 and −0.1383), which were set at the average of −0.138 for both odd and even n series of **1A[*n*]**. The value for the pre-exponential factor c for

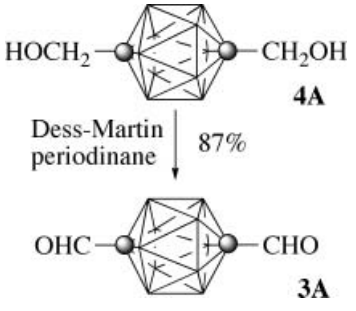

Scheme 2.

Table 1. Transition temperatures (°C) and enthalpies (kJ mol^{-1}) for series **1A[*n*]** and **1B[*n*]**.[a]

1[n]

$\mathcal{A}$	**A**	**B**
		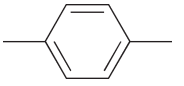
n		
1	Cr 207 N 211.9 I 28.8 2.9	Cr 226 N 343.5 I[b,c] 49.3 1.5[d]
2	Cr 218 (N 212.2) I 51.5 2.8	Cr_1 196 Cr_2 198 N 336 I[b,e] 38.6[f] 1.0
3	Cr 189 (N 165)[g] I 32.4	Cr 207 N 306.2 I[b,h] 43.1 2.0
4	Cr 152 N 160.3 I 28.8 3.3	Cr 191 SmC 221N 295.5 I[i,j]
5	Cr 137 (N 129.3) I 40.3 2.6	Cr_1 89 Cr_2 174 SmI 178 SmC 223 SmA 234 N 272.5 I[k] 10.8 28.9 3.9 0.2 0.6 2.0
6	Cr 137 (N 123.6) I 44.8 3.2	Cr 159 SmI[l] 176 SmC 232 SmA 239 N 262 I[i]
7	Cr 133 (N 107)[g] I 44.7	Cr_1 124 Cr_2 151 (SmF 151) SmI 175 SmC 231 SmA 235 N 249.6 I 28.0 32.9 0.04 4.9 1.1 0.5 2.2
8	Cr 125 (N 104.8) I 53.0 3.1	Cr 144 SmI[l] 172 SmC 234 SmA 241 N 246 I[i]
9	Cr 107 (N 95.5) I 46 2.9	Cr 138 (SmF 134)[g] SmI 172 SmC 224[g] SmA 227 N 232.7 I 83.4 5.2 0 2.0 2.6
10	Cr 101 (N 93.7) I 48.6 3.1	Cr_1 134 Cr_2 137 SmI 170 SmC 222[g] SmA 224 N 226.7 I 31.3 23.1 5.4 0 3.2 3.1

[a] Cr=crystal, Sm=smectic, N=nematic, I=isotropic.
[b] 20°C min^{-1} scanning rate.
[c] Cr 224 N 330 I [13], [14].
[d] Partial sublimation, enthalpy approximated.
[e] Cr 198 N 323 I [13].
[f] Combined enthalpy of Cr–Cr transition and melting.
[g] From microscopic observations.
[h] Cr 206 N 298 I [13].
[i] [12].
[j] Cr 190 M 287 I [13].
[k] Cr 90 Sm_1 175 Sm_2 223 Sm_3 232 N 268 I [15].
[l] Previously SmB was postulated [12]. See text for details.

both series of **1B[*n*]** was set at −0.095. The resulting 1-parameter fitting functions are shown in figure 2.

The established parameters a and d for functions describing the trend in the T_{NI} represent the upper limits. As we demonstrated for a more extensive homologous series [6], these values asymptotically approach a lower limit for $n\rightarrow\infty$. Nevertheless, they offer a useful comparison of both series and verification

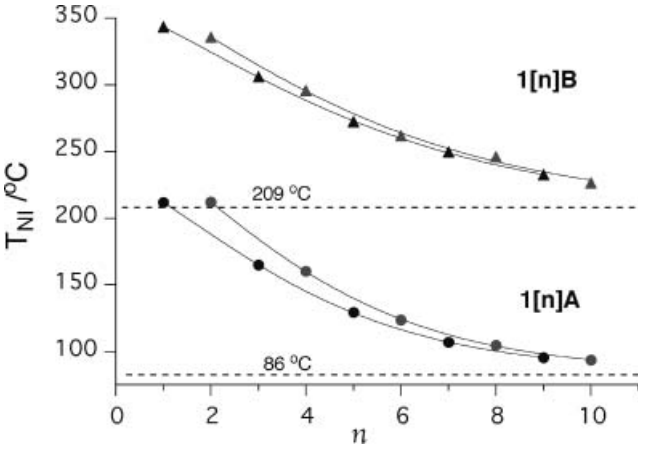

Figure 2. Nematic–isotropic transition temperatures T_{NI} for **1A[*n*]** and **1B[*n*]** as a function of the chain length *n*. Best fit 1-parameter functions: **1A[*n*]** $T_{NI}=86+\exp(4.975-0.138\times n\hat{}1.35)$ for odd n and $T_{NI}=86+\exp(5.193-0.138\times n\hat{}1.35)$ for even *n*; **1B[n]** $T_{NI}=209+\exp(4.996-0.095\times n\hat{}1.35)$ for odd *n*, and $T_{NI}=209+\exp(5.082-0.095\times n\hat{}1.35)$ for even *n*. $\mathcal{R}^2$ for **1A[*n*]** and odd *n* **1B[*n*]** is >0.999; for even *n* **1B[*n*]** $\mathcal{R}^2=0.997$.

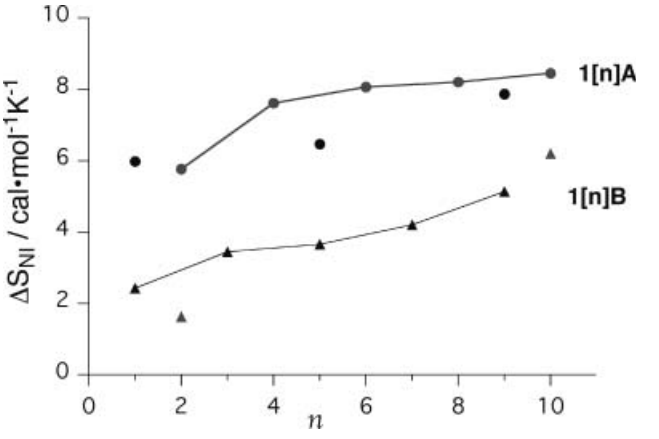

Figure 3. Entropy change ΔS_{NI} at the nematic–isotropic transition for **1A[*n*]** and **1B[*n*]** as a function of the chain length *n*. The lines are guides for the eye.

of internal consistency within each homologous series. Thus, the apparent range for the T_{NI} values in the series or the difference between T_{NI} for **1[1]** and for **1[∞]** is similar for both series: 126°C for series **A** and 134°C for series **B**. Further comparison of the fitting functions shows a ~40% larger coefficient *c* for the 12-vertex carborane series **A** ($c=-0.138$) than for the benzene analogues **B** ($c=-0.095$), which results in a steeper descent of the T_{NI} in the homologous series.

Analysis of the entropy change for the nematic–isotropic transition revealed significantly higher values for the carborane derivatives **A** than for their benzene analogues **B**. Figure 3 shows a comparison of ΔS_{NI} for the complete series of **1A[*n*]** for even *n* and **1B[*n*]** for odd *n*. Entropy changes for **1A[3]** and **1A[7]** could not be obtained since the samples crystallized before the appearance of the monotropic nematic phase during the DSC analysis. The observed higher ΔS_{NI} values for series **1A[*n*]** suggest greater conformational changes in the carborane derivatives during the phase transition than in the benzene derivatives **1B[*n*]**. Support for this is provided by conformational analysis of carborane-1-carbaldehyde and benzaldehyde, models for the azomethine derivatives. Computational results [17] show about a six times lower barrier to internal rotation around the ring–CHO bond in the former than in benzaldehyde [18] (figure 4). Such a low barrier to rotation in this and other carborane derivatives (e.g. [6]) results from a high axis of rotation (C_5), low steric hindrance, and low degree of electronic coupling between carborane and the substituent, as apparent from the UV spectrum of **1A[5]** (*vide infra*). In consequence, carborane derivatives have a larger number of shallow conformational minima, which give rise to excessive conformational mobility in the centre of the molecule and a low dynamic aspect ratio. This results in high entropy of transition and low mesophase stability as evident from the observed relatively low T_{NI} values and their steep descent in the carborane series **1A[*n*]**.

The effect of substitution of the linking oxygen atom with a methylene group was briefly investigated, and three members of a homologous series of carborane derivatives **2A[*n*]** with $n=5$–7 were prepared. DSC analysis showed only melting and crystallization transitions, while monotropic nematic phases were observed by microscope in supercooled micro-droplets (table 2). All three compounds show nematic phases significantly destabilized relative to the alkoxy analogues **1A[*n*]**. The difference in the T_{NI} is 96°C for **1A[4]**–**2A[5]** and **1A[5]**–**2A[6]** pairs, and 80°C for the **1A[6]**–**2A[7]** pair. For comparison, the same replacement of O in the benzene derivatives **1B[*n*]** with a CH_2 group in **2B[*n*]**[19] for the same *n* results in depression of the T_{NI} by about 60°C and the induction of a very rich smectic polymorphism. This significant difference in the degree of destabilization of the nematic phase in the carborane and benzene analogues may be related to the greater importance of the quadrupolar interactions between the carborane

Figure 4. Calculated (MP2/6–316(*d*)) free energy of activation to internal rotation around the ring–CHO bond [17].

Table 2. Transition temperatures (°C) and enthalpies (kJ mol^{-1}) (in brackets) for **2A[*n*]**.[a]

2A[n]

n	Transitions
5	Cr 141 (N 64) I 48.0
6	Cr 105 (N 33) I 37.2
7	Cr 105 (N 45) I 43.2

[a] Cr=crystal, N=nematic, I=isotropic. The N-I transition temperatures were obtained from microscopic observations.

cage and the alkoxyphenyl ring [3, 20], than between the phenyl and alkoxyphenyl rings.

Of the ten benzene derivatives **1B[*n*]** used for comparison with the carborane series **1A[*n*]**, seven have been described in the literature, mainly by two research groups [12, 13]. Their polymorphism, however, was only partially characterized, and there are significant discrepancies in the reported transition temperatures. For exapmple, clearing temperatures reported for **1B[1]** and **1B[4]** by one group [12] are higher by 10°C and 14°C, respectively, than the values in the earlier report [13]. The higher clearing temperature for **1B[4]** was confirmed [21], and the lower T_{NI} of 330°C for **1B[1]** is consistent with another report [14]. This suggests that while the transition temperatures for **1B[4]** and higher homologues [12] are likely to be correct, those reported earlier [13] for **1B[1]**–**1B[3]** could be underestimated by up to 10°C. Such large uncertainties, especially for the first members of the series, would not permit the numerical analysis of the T_{NI} trends shown in figure 2. Therefore, to complete the series and to obtain accurate and consistent T_{NI} values for the odd *n* series of mesogens, we prepared the three previously unknown derivatives **1B[7]**, **1B[9]** and **1B[10]**, and also four previously reported derivatives **1B[1]**–**1B[3]**[13] and **1B[5]**[15].

Analysis of **1B[2]**–**1B[3]** showed only nematic behaviour, which is consistent with the literature data [13, 22], but with significantly higher transition temperatures than previously reported (table 1). During analysis, we observed decomposition accompanied by sublimation of the samples at the low heating rates (5°C min^{-1}). This is certainly a potential source of the discrepancies in the literature T_{NI} values. The relatively narrow (about 1°C) isotropization peaks were recorded at 20°C min^{-1} heating rates.

Investigations of the higher homologues **1B[5]**, **1B[7]**, **1B[9]** and **1B[10]** revealed rich polymorphism as shown

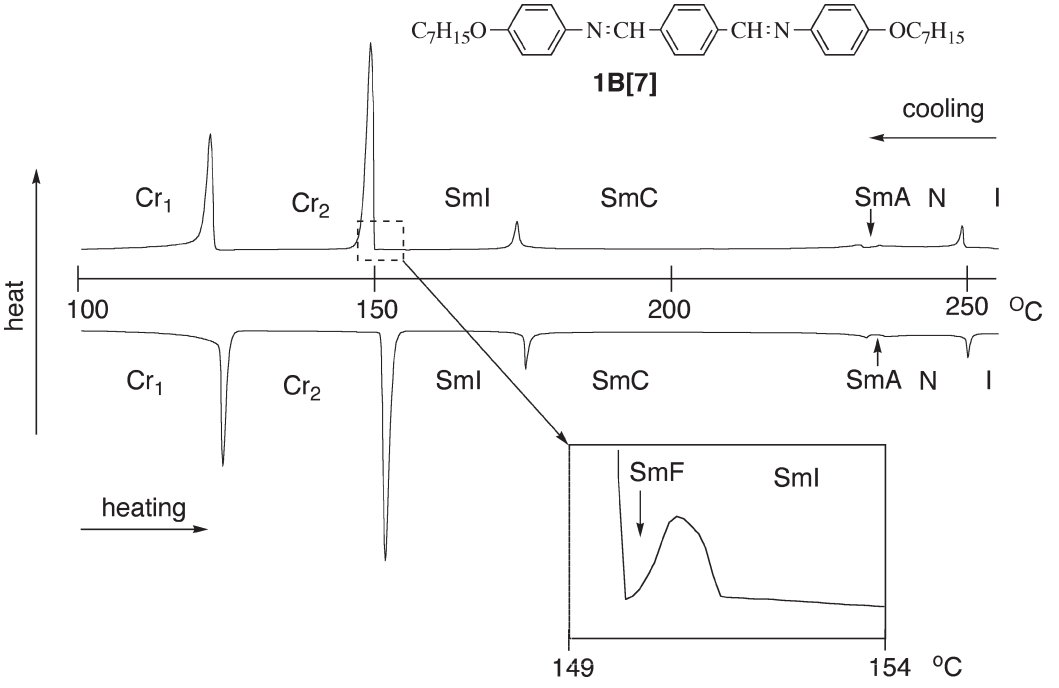

Figure 5. A DSC trace for **1B[7]** obtained on heating (lower trace) and on cooling (upper trace) at a scanning rate of 5°C min^{-1}. The expanded region of 149–154°C is shown in the inset.

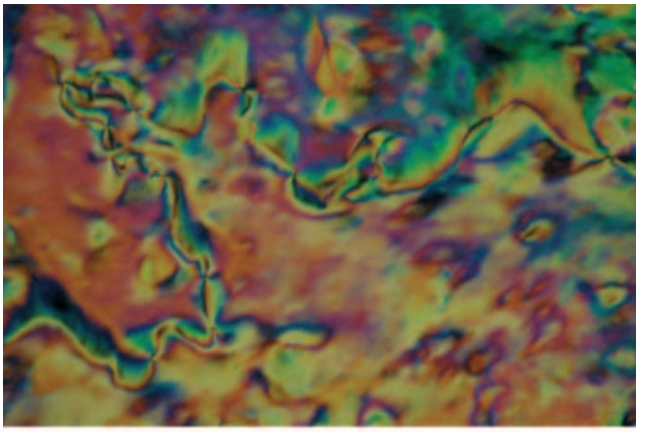

(*a*)

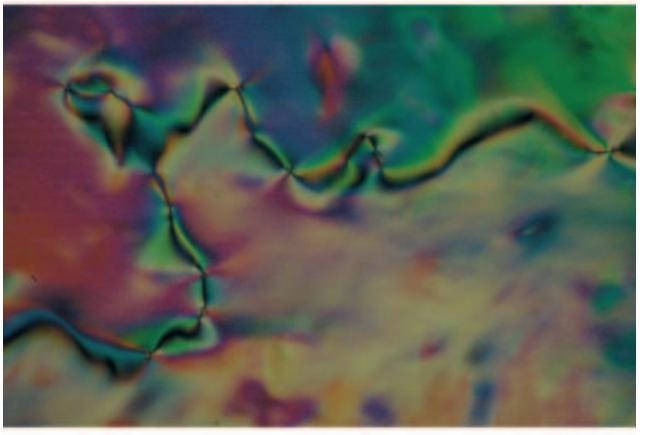

(*b*)

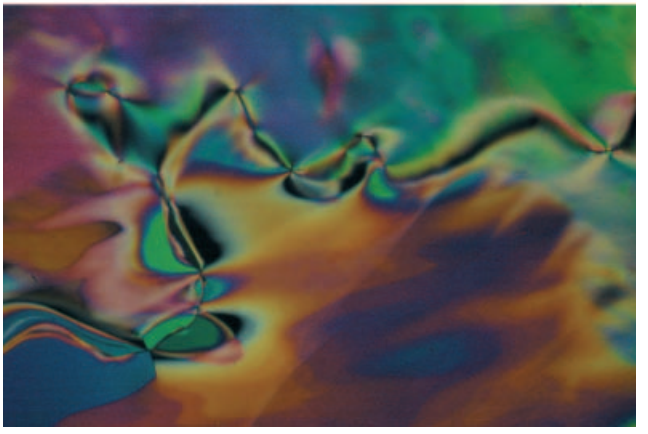

(*c*)

Figure 6. Natural schlieren textures observed in polarized light for **1B[7]** in the same sample region: (*a*) SmC phase at 180°C, (*b*) SmI at 165°C, (*c*) SmF near the phase transition at 150°C. Magnification 60×.

for **1B[7]** in figure 5. Polarizing microscopy analysis established that all four homologues exhibit the SmI–SmC–SmA–N phase sequence. In addition, a narrow range monotropic SmF was found for **1B[7]** and **1B[9]**. The SmA phase was identified based on the formation of the characteristic focal-conic fan-shaped optical textures in small areas of generally homeotropically oriented samples. On cooling, the black homeotropic regions formed a schlieren texture typical for the SmC phase as shown for **1B[7]** in figure 6 (*a*). Further cooling resulted in a transformation to a homomorphic Schlieren texture characteristic for SmI, figure 6 (*b*). In the case of **1B[7]** and **1B[9]**, another lower temperature schlieren texture homomorphic with the SmC texture was found and identified as the SmF phase, figure 6 (*c*). None of the investigated compounds showed a mosaic texture.

Our results for the four higher homologues of **1B[*n*]** are in part consistent with the previously postulated sequence SmC–SmA–N for **1B[6]** and **1B[8]** [12]. The phase below the SmC in **1B[6]** and **1B[8]** was previously suggested to be a SmB phase based on molecular similarities and phase behaviour in a series of phenylene-1,4-diamine analogues [12]. However, our results and the general trends in homologous series indicate that these phases should be reassigned to SmI.

2.3. *Absorption spectroscopy*

For a better understanding of the electronic interactions between the carborane cluster and π substituents, we recorded UV spectra for two representative compounds and analysed them using quantum-mechanical methods. The observed spectrum for **1B[5]** (figure 7) is consistent with that reported for **1B[1]** and **1B[2]** in dioxane [23]. Previously, only one broad long wavelength absorption band was observed at about 375 nm. In the present case the band appears to exhibit vibronic structure and

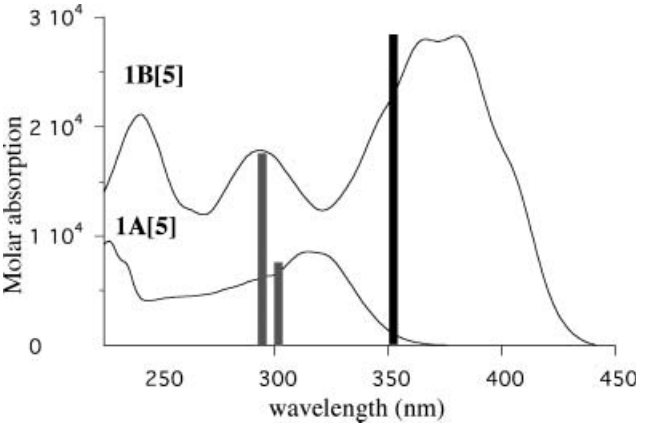

Figure 7. Electronic absorption spectra for carborane **1A[5]** and benzene derivative **1B[5]** in cyclohexane. Vertical bars (grey for **1A[5]** and black for **1B[5]**) represent the oscillator strength of the longest wavelength transition scaled by 1.5×10^4.

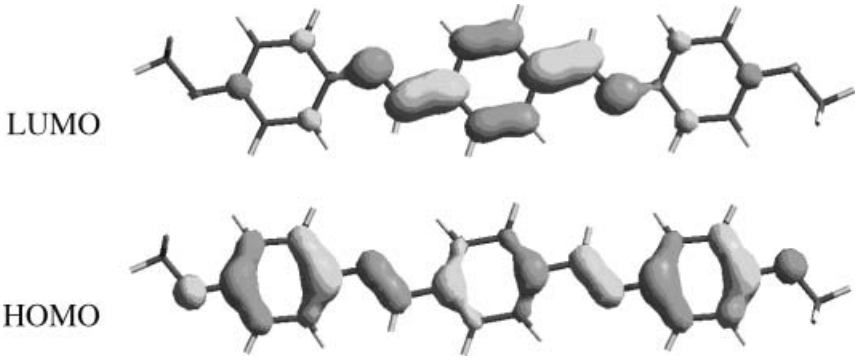

Figure 8. HOMO (lower) and LUMO (upper) contours calculated (ZINDO//HF-6-31(d)) for **1B[1]** at the C_{2h} geometry.

consists of two maxima at 380 and 367 nm, and two shoulder features on each side of the band.

Analysis of ZINDO results for the methoxy derivatives **1A[1]** and **1B[1]** at the C_{2h} geometry revealed that the longest wavelength absorption in the latter has a longitudinal transition moment and originates from the HOMO–LUMO and, to lesser extent, HOMO-1–LUMO+1 excitations. Electronic absorption spectra were calculated using using ZINDO (INDO/2 method, maxCI = 500, convergence limit = 10^{-5}, all active (valence) orbitals included in the CI) in the Cerius2 suite of programs using the HF/6-31G*-optimized geometry at the C_{2h} symmetry. The HOMO of **1B[1]** is delocalized over the entire π-system and the LUMO is largely localized on the terephthaldehyde imine part (figure 8). In contrast, the HOMO-1 and LUMO+1 are mainly localized on the aniline part.

Analysis for the carborane derivative **1A[1]** revealed a much more complex origin of the low energy portion of the UV spectrum. ZINDO calculations show two closely spaced absorption bands at 303 and 296 nm with an oscillator strength f of 0.51 and 1.18, respectively. Both involve different combinations of the same four excitations from HOMO-1 to LUMO+4 and LUMO+10, and HOMO to LUMO+2, and LUMO+9. The HOMO-1 and HOMO orbitals are separated by 0.11 eV (ZINDO) and can be described as antisymmetric and symmetric combinations of orbitals localized on each aniline ring, as illustrated for the HOMO in figure 9. The unoccupied orbitals involved in the low energy electronic transitions are mainly localized on the aromatic part, as is shown for LUMO+4 in figure 9. The only orbital active in this transition that involves the carborane cage is LUMO+2. In contrast, the LUMO and LUMO+1 are solely localized on the carborane cage and do not participate in these low energy transition processes. Interestingly, LUMO+9 and LUMO+10 are symmetric and antisymmetric combinations of orbitals localized on the benzene rings and separated by 0.002 eV (ZINDO).

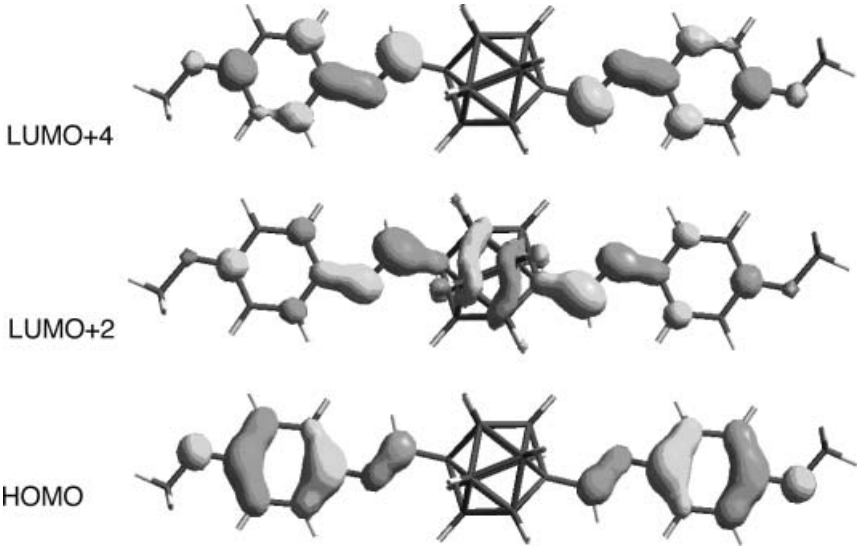

Figure 9. MO contours calculated (ZINDO//HF-6-31(d)) for **1A[1]** at the C_{2h} geometry.

3. Conclusions

Analysis of two homologous series shows lower stability of nematic phases, steeper descent of the T_{NI} in the series, and higher entropy change for the clearing transition in the carborane derivatives **1A[*n*]** relative to the analogous benzene series **1B[*n*]**. These differences are attributed to the markedly lower barrier to internal rotation around the ring–CH= bond and consequently higher molecular flexibility and lower dynamic aspect ratio in the carborane derivatives **1A[*n*]** than in the benzene analogs **1B[*n*]**. The calculated barrier to internal rotation in the carborane derivatives is consistent with the relatively low degree of electronic interaction between the cage and the π system in **1A**, as is evident from the electronic absorption spectra.

The high correlation factor and low error on parameters used in the numerical approximation of the T_{NI} values demonstrates the internal consistency of the datapoints and hence purity of the compounds and accuracy of the measurements. It also provides a useful quantitative measure of the ring effect on nematic phase stability.

Replacement of an oxygen atom in **1A** with a methylene group in **2A** results in about 30°C stronger destabilization of the nematic phase than in the analogous benzene derivatives. This is attributed to the importance of the carborane–alkoxyphenyl ring quadrupolar stabilizing interactions in **1A** which are absent in **1B**.

4. Experimental Section

4.1. *Characterzation*

NMR spectra were obtained at 270 MHz (^{1}H) or 67.8 MHz (^{13}C) field in $CDCl_3$ and referenced to TMS unless stated otherwise. UV spectra were measured in cyclohexane and molar absorptions were obtained using Beers law for the 315 and 380 nm bands in **1A[5]** and **1B[5]**, respectively. Elemental analysis was provided by Instrumental Analysis Center for Chemistry, Graduate School of Science, Tohoku University or by Atlantic Microlab, GA. *p*-Carborane was purchased from Katchem s. r. o. (Prague, Czech Republic). Other chemicals were purchased from Aldrich or Tokyo Kasei Ltd. 4-Nonyloxy [24] and 4-decyloxyanilne [25] were prepared according to a general literature procedure [26].

Optical microscopy and phase identification was performed using a PZO 'Biolar' polarizing microscope equipped with a HCS250 Instec hot stage. Thermal analysis was obtained using a TA Instruments 2920 DSC. Transition temperatures (onset) and enthalpies were obtained using small samples (1–2 mg) and a heating rate of 5°C min^{-1} under a flow of nitrogen. For DSC and microscopic analyses, each compound was rigorously purified by dissolving in CH_2Cl_2, filtering to remove particles, evaporating and repeated recrystallization from indicated solvent until constant transition temperature. The resulting crystals were dried in vacuum overnight at ambient temperature. For such purified samples, the clearing transition was typically less than 0.3°C wide.

4.2. *Preparation of Schiff's bases 1A[n] and 2A[n]: general procedure*

A solution of 1,12-dicarba-*closo*-dodecaborane-1,12-dicarboxaldehyde (**3A**, 200 mg, 1 mmol), the appropriate aniline (2.2 mmol, 2.2 equiv.) and a catalytic amount of *p*-toluenesulphonic acid in anhydrous toluene (5 ml) was heated under reflux for 1 h, water being removed with the aid of a Dean–Stark trap. The mixture was poured into a saturated aqueous solution of $NaHCO_3$ and the mixture extracted with AcOEt. The organic layer was washed with brine, dried over $MgSO_4$ and concentrated under reduced pressure. The crude product was purified either by column chromatography (silica gel, 20/1 *n*-hexane/AcOEt) and recrystallization from *n*-hexane containing CH_2Cl_2 (**1A[6]**–**1A[10]** and **2A[5]**–**2A[7]**) or by recrystallization alone to give the colourless crystalline pure product.

4.2.1. 1,12-Bis(4-methoxyphenylimiomethyl)-*p*-carborane, 1A[1]. Prisms (toluene), yield 60%. ^{1}H NMR δ 1.50–3.75 (brm, 10H), 3.79 (s, 6H), 6.83 (d, J=8.9 Hz, 4H), 6.86 (d, J=8.9 Hz, 4H), 7.32 (s, 2H). ^{13}C NMR δ 55.5, 80.9, 114.2, 122.1, 142.1, 153.0, 158.8. HRMS: calcd for $C_{18}H_{26}B_{10}N_2O_2$ 410.2997; found 410.3001. Anal: calcd for $C_{18}H_{26}B_{10}N_2O_2$ C 52.66, H 6.38, N 6.82; found C 52.74, H 6.30, N 6.76%.

4.2.2. 1,12-Bis(4-ethoxyphenylimiomethyl)-*p*-carborane, 1A[2]. Prisms (toluene), yield 60%. ^{1}H NMR δ 1.39 (t, J=7.0 Hz, 6H), 1.50–3.75 (brm, 10H), 4.00 (q, J=7.0 Hz, 4H), 6.82 (d, J=8.9 Hz, 4H), 6.96 (d, J=9.2 Hz, 4H), 7.32 (s, 2H). ^{13}C NMR δ 14.7, 63.6, 80.7, 114.6, 122.0, 141.8, 152.8, 158.1. HRMS: calcd for $C_{20}H_{30}B_{10}N_2O_2$ 438.3310; found 438.3320. Anal: calcd for $C_{20}H_{30}B_{10}N_2O_2$ C 54.77, H 6.89, N 6.39; found C 54.51, H 6.69, N 6.26%.

4.2.3. 1,12-Bis(4-propoxyphenylimiomethyl)-*p*-carborane, 1A[3]. Needles (toluene), yield 58%. ^{1}H NMR δ 1.02 (t, J=7.3 Hz, 6H), 1.50–3.75 (brm, 10H), 1.79 (sext., J=7.1 Hz, 4H), 3.89 (t, J=6.6 Hz, 4H), 6.82 (d, J=8.9 Hz, 4H), 6.96 (d, J=9.2 Hz, 4H), 7.32 (s, 2H).

^{13}C NMR δ 10.6, 22.6, 69.8, 80.9, 114.8, 122.1, 141.9, 152.8, 158.4. HRMS: calcd for $C_{22}H_{34}B_{10}N_2O_2$ 466.3623; found 466.3618. Anal: calcd for $C_{22}H_{34}B_{10}N_2O_2$ C 56.63, H 7.34, N 6.00; found C 56.88, H 7.14, N 6.04%.

4.2.4. 1,12-Bis(4-butoxyphenylimiomethyl)-*p*-carborane, 1A[4]. Needles (*n*-hexane), yield 65%. ^{1}H NMR δ 0.96 (t, J=7.6 Hz, 6H), 1.47 (sext., J=7.6 Hz, 4H), 1.50–3.75 (brm, 10H), 1.75 (quint., J=7.1 Hz, 4H), 3.93 (t, J=6.6 Hz, 4H), 6.82 (d, J=8.9 Hz, 4H), 6.96 (d, J=9.2 Hz, 4H), 7.32 (s, 2H). ^{13}C NMR δ 13.8, 19.2, 31.2, 67.9, 80.7, 114.7, 122.0, 141.8, 152.7, 158.3. HRMS: calcd for $C_{24}H_{38}B_{10}N_2O_2$ 494.3936; found 494.3917. Anal: calcd for $C_{24}H_{38}B_{10}N_2O_2$ C 58.27, H 7.74, N 5.66; found C 58.27, H 7.57 N, 5.59%.

4.2.5. 1,12-Bis(4-pentyloxyphenylimiomethyl)-*p*-carborane, 1A[5]. Prisms (*n*-hexane), yield 92%. ^{1}H NMR δ 0.92 (t, J=7.0 Hz, 6H), 1.30–1.50 (m, 8H), 1.50–3.75 (brm, 10H), 1.76 (quint., J=7.0 Hz, 4H), 3.92 (t, J=6.6 Hz, 4H), 6.82 (d, J=8.9 Hz, 4H), 6.96 (d, J=8.9 Hz, 4H), 7.32 (s, 2H). ^{13}C NMR δ 14.1, 22.5, 28.2, 29.0, 68.2, 80.9, 114.7, 122.1, 141.8, 152.7, 158.4. UV (cyclohexane), λ_{max} (log ε) 315 (3.93), 297 sh (3.80), 259 sh (3.65), 227 (3.98). HRMS: calcd for $C_{26}H_{42}B_{10}N_2O_2$ 522.4249; found 522.4249. Anal: calcd for $C_{26}H_{42}B_{10}N_2O_2$ C 59.74, H 8.10, N 5.36; found C 59.88, H 8.15, N 5.36%.

4.2.6. 1,12-Bis(4-hexyloxyphenylimiomethyl)-*p*-carborane, 1A[6]. Needles (*n*-hexane), yield 80%. ^{1}H NMR δ 0.90 (t, J=6.9 Hz, 6H), 1.20–1.50 (m, 12H), 1.50–3.75 (brm, 10H), 1.76 (quint., J=7.0 Hz, 4H), 3.92 (t, J=6.6 Hz, 4H), 6.82 (d, J=8.9 Hz, 4H), 6.96 (d, J=8.9 Hz, 4H), 7.32 (s, 2H). ^{13}C NMR δ 14.1, 22.6, 25.7, 29.2, 31.6, 68.2, 80.9, 114.7, 122.1, 141.8, 152.7, 158.4. HRMS: calcd for $C_{28}H_{46}B_{10}N_2O_2$ 550.4562; found 550.4532. Anal: calcd for $C_{28}H_{46}B_{10}N_2O_2$ C 61.06, H 8.42, N 5.09; found C 61.31, H 8.50 N 5.18%.

4.2.7. 1,12-Bis(4-heptyloxyphenylimiomethyl)-*p*-carborane, 1A[7]. Needles (*n*-hexane), yield 91%. ^{1}H NMR δ 0.89 (t, J=6.8 Hz, 6H), 1.20–1.50 (m, 16H), 1.50–3.75 (brm, 10H), 1.76 (quint., J=6.9 Hz, 4H), 3.92 (t, J=6.5 Hz, 4H), 6.81 (d, J=8.9 Hz, 4H), 6.96 (d, J=8.9 Hz, 4H), 7.32 (s, 2H). ^{13}C NMR δ 14.2, 22.6, 26.0, 29.1, 29.3, 31.8, 68.2, 80.9, 114.7, 122.1, 141.8, 152.7, 158.4. HRMS: calcd for $C_{30}H_{50}B_{10}N_2O_2$ 578.4875; found 578.4897. Anal: calcd for $C_{30}H_{50}B_{10}N_2O_2$ C 62.25, H 8.71, N 4.84; found C 62.41, H 8.71, N 4.86%.

4.2.8. 1,12-Bis(4-octyloxyphenylimiomethyl)-*p*-carborane, 1A[8]. Needles (*n*-hexane), yield 74%. ^{1}H NMR δ 0.88 (t, J=6.8 Hz, 6H), 1.20–1.50 (m, 20H), 1.50–3.75 (brm, 10H), 1.76 (quint., J=6.9 Hz, 4H), 3.92 (t, J=6.5 Hz, 4H), 6.82 (d, J=8.9 Hz, 4H), 6.96 (d, J=8.9 Hz, 4H), 7.32 (s, 2H). ^{13}C NMR δ 14.2, 22.7, 26.1, 29.3, 29.4, 31.8, 68.2, 80.9, 114.7, 122.1, 141.8, 152.7, 158.4. HRMS: calcd for $C_{32}H_{54}B_{10}N_2O_2$ 606.5189; found 606.5200. Anal: calcd for $C_{32}H_{54}B_{10}N_2O_2$ C 63.33, H 8.97; found C 63.35, H 9.04%.

4.2.9. 1,12-Bis(4-nonyloxyphenylimiomethyl)-*p*-carborane, 1A[9]. Cotton-like (*n*-hexane), yield 96%. ^{1}H NMR δ 0.88 (t, J=6.6 Hz, 6H), 1.20–1.50 (m, 24H), 1.50–3.75 (brm, 10H), 1.76 (quint., J=7.0 Hz, 4H), 3.92 (t, J=6.6 Hz, 4H), 6.82 (d, J=8.9 Hz, 4H), 6.96 (d, J=8.9 Hz, 4H), 7.32 (s, 2 H). 13C NMR δ 14.2, 22.6, 26.0, 29.17, 29.20, 29.4, 29.5, 31.8, 68.2, 80.9, 114.8, 122.2, 141.9, 152.8, 158.6. HRMS: calcd for $C_{34}H_{58}B_{10}N_2O_2$ 634.5502; found 634.5508. Anal: calcd for $C_{34}H_{58}B_{10}N_2O_2$ C 64.32, H 9.21; found C 64.24, H 9.27%.

4.2.10. 1,12-Bis(4-decyloxyphenylimiomethyl)-*p*-carborane, 1A[10]. Cubes (*n*-hexane), yield 85%. ^{1}H NMR δ 0.88 (t, J=6.8 Hz, 6H), 1.20–1.50 (m, 28H), 1.50–3.75 (brm, 10H), 1.76 (quint., J=6.9 Hz, 4H), 3.92 (t, J=6.6 Hz, 4H), 6.82 (d, J=8.9 Hz, 4H), 6.96 (d, J=8.9 Hz, 4H), 7.32 (s, 2H). ^{13}C NMR δ 14.1, 22.7, 29.2, 29.32, 29.38, 29.5, 31.9, 68.3, 114.9, 122.2, 142.0, 153.0, 158.6. HRMS: calcd for $C_{36}H_{62}B_{10}N_2O_2$ 662.5814; found 662.5819. Anal: calcd for $C_{36}H_{62}B_{10}N_2O_2$ C 65.22, H 9.43; found C 65.41, H 9.43%.

4.2.11. 1,12-Bis(4-pentylphenylimiomethyl)-*p*-carborane, 2A[5]. Needles (*n*-heptane), yield 90%. ^{1}H NMR δ 0.87 (t, J=6.8 Hz, 6H), 1.21–1.38 (m, 8H), 1.50–3.75 (brm, 10H), 1.56 (quint., J=7.4 Hz, 4H), 2.56 (t, J=7.7 Hz, 4H), 6.88 (d, J=8.4 Hz, 4H), 7.11 (d, J=8.4 Hz, 4H), 7.32 (s, 2H). ^{13}C NMR δ 14.1, 22.6, 31.2, 31.4, 35.4, 80.8, 120.5, 128.9, 141.9, 146.8, 154.2. HRMS: calcd for $C_{26}H_{42}B_{10}N_2$ 490.4351; found 490.4381. Anal: calcd for $C_{26}H_{42}B_{10}N_2$ C 63.63, H 8.63, N 5.71; found C 63.66, H, 8.46, N 5.69%.

4.2.12. 1,12-Bis(4-hexylphenylimiomethyl)-*p*-carborane, 2A[6]. Prisms (*n*-pentane), yield 83%. ^{1}H NMR δ 0.87 (t, J=6.6 Hz, 6H), 1.20–1.40 (m, 12H), 1.50–3.75 (brm, 10H), 1.56 (quint., J=7.2 Hz, 4H), 2.57 (t, J=7.7 Hz, 4H), 6.88 (d, J=8.2 Hz, 4H), 7.11 (d, J=8.2 Hz, 4H), 7.32 (s, 2H). ^{13}C NMR δ 14.0, 22.5, 28.8, 31.4, 31.6,

35.4, 80.7, 120.4, 128.8, 141.8, 146.7, 154.2. HRMS: calcd for $C_{28}H_{46}B_{10}N_2$ 518.4664; found 518.4670. Anal: calcd for $C_{28}H_{46}B_{10}N_2$ C 64.82, H 8.94, N 5.40; found C 64.61, H 8.84, N 5.37%.

4.2.13. 1,12-Bis(4-heptylphenylimiomethyl)-*p*-carborane, 2A[7]. Prisms (*n*-pentane), yield 89%. ^{1}H NMR δ 0.87 (t, J=6.8 Hz, 6H), 1.18–1.35 (m, 16H), 1.50–3.75 (brm, 10H), 1.56 (quint., J=7.2 Hz, 4H), 2.56 (t, J=7.6 Hz, 4H), 6.88 (d, J=8.4 Hz, 4H), 7.11 (d, J=8.4 Hz, 4H), 7.32 (s, 2H). ^{13}C NMR δ 14.1, 22.6, 29.0, 29.1, 31.4, 31.7, 35.4, 80.7, 120.4, 128.8, 141.8, 146.7, 154.2. HRMS: calcd for $C_{30}H_{50}B_{10}N_2$ 546.4977; found 546.4964. Anal: calcd for $C_{30}H_{50}B_{10}N_2$ C 65.89, H 9.22, found C 66.05, H 9.24%.

4.3. *Preparation of Terephthaldehyde Schiff bases 1B[n]: general procedure*

A solution of terephthaldehyde (200 mg, 1.49 mmol), the appropriate aniline (3.0 mmol, 2.0 equiv.) and a catalytic amount of *p*-toluenesulphonic acid in anhydrous toluene (5 ml) was heated under reflux using a Dean–Stark water trap for 12 h. The resulting mixture was poured into a saturated aqueous solution of $NaHCO_3$, and AcOEt was added. Insoluble material was collected and recrystallized from AcOEt to give the pure product as light yellow leaflets.

4.3.1. 1,4-Bis(4-methoxyphenylimiomethyl)benzene, 1B[1]. Crystallized (plates from *o*-$C_6H_4Cl_2$) and sublimed (280°C/0.1 Torr). ^{1}H NMR δ 3.83 (s, 6H), 6.93 (d, J=8.9 Hz, 4H), 7.26 (d, J=8.9 Hz, 4H), 7.97 (s, 4H), 8.52 (s, 2H). Anal: calcd for $C_{22}H_{20}N_2O_2$ C 76.72, H 5.85, N 8.13; found C 76.70, H 8.22, N 5.86%.

4.3.2. 1,4-Bis(4-ethoxyphenylimiomethyl)benzene, 1B[2]. Yield 95%; light yellow leaflets (AcOEt). ^{1}H NMR δ 1.44 (t, J=6.9 Hz, 6H), 3.96 (t, J=6.6 Hz, 4H), 6.94 (d, J=8.9 Hz, 4H), 7.26 (d, J=8.9 Hz, 4H), 7.98 (s, 4H), 8.54 (s, 2H). ^{13}C NMR δ 14.9, 63.7, 115.0, 122.4, 128.9, 138.6, 144.4, 157.2, 158.0. MS, *m*/*z* 372 (M^+, 100). Anal: calcd for $C_{24}H_{24}N_2O_2$ C 77.39 H 6.49, N 7.52; found C 77.51, H 6.76, N 7.56%.

4.3.3. 1,4-Bis(4-propoxyphenylimiomethyl)benzene, 1B[3]. Yield 91%, light yellow leaflets (AcOEt). ^{1}H NMR δ 1.06 (t, J=7.4 Hz, 6H), 1.83 (sext., J=7.0 Hz, 4H), 4.07 (t, J=7.0 Hz, 4H), 6.94 (d, J=8.9 Hz, 4H), 7.27 (d, J=8.9 Hz, 4H), 7.98 (s, 4H), 8.54 (s, 2H). ^{13}C NMR δ 10.5, 22.6, 69.8, 115.0, 122.3, 128.9, 138.6, 144.4, 157.2, 158.2. MS, *m*/*z* 400 (M^+, 100). Anal: calcd for $C_{26}H_{28}N_2O_2$ C 77.97, H 7.05, N 6.99; found C 78.04, H 7.26, N 7.04%.

4.3.4. 1,4-Bis(4-pentyloxyphenylimiomethyl)benzene, 1B[5]. Yield 71%. ^{1}H NMR δ 0.94 (t, J=7.2 Hz, 6H), 1.30–1.55 (m, 8H), 1.81 (quint., J=7.0 Hz, 4H), 3.98 (t, J=6.6 Hz, 4H), 6.93 (d, J=8.9 Hz, 4H), 7.26 (d, J=8.9 Hz, 4H), 7.97 (s, 4H), 8.53 (s, 2H). ^{13}C NMR δ 14.0, 22.4, 28.2, 29.0, 68.2, 114.8, 122.1, 128.6, 138.4, 144.1, 156.9, 157.9. UV (cyclohexane), λ_{max} (log ε) 380 (4.45), 367 (4.45), 294 (4.25), 241 (4.32). HRMS: calcd for $C_{30}H_{36}N_2O_2$ 456.2777; found 456.2765. Anal: calcd for $C_{30}H_{36}N_2O_2$ C 78.91, H 7.95, N 6.13; Found C 78.63, H 8.04, N 6.18%.

4.3.5. 1,4-Bis(4-heptyloxyphenylimiomethyl)benzene, 1B[7]. Yield 63%. ^{1}H NMR δ 0.94 (t, J=7.2)(Hz, 6H), 1.30–1.55 (m, 16H), 1.80 (quint., J=7.0(Hz, 4H), 3.98 (t, J=6.5 Hz, 4H), 6.93 (d, J=8.9)(Hz, 4H), 7.26 (d, J=8.6 Hz, 4H), 7.98 (s, 4H), 8.53 (s, 2H). ^{13}C NMR δ 14.2, 22.7, 26.1, 29.2, 29.4, 31.9, 68.3, 114.9, 122.2, 128.7, 138.5, 144.3, 157.0, 158.0. HRMS: calcd for $C_{34}H_{44}N_2O_2$ 512.3403; found 512.3430. Anal: calcd for $C_{34}H_{44}N_2O_2$ C 79.65, H 8.65, N 5.46; found C 79.36, H 8.74, N 5.39%.

4.3.6. 1,4-Bis(4-nonyloxyphenylimiomethyl)benzene, 1B[9]. Yield 43%; light yellow leaflets (AcOEt): ^{1}H NMR δ 0.89 (t, J=6.8 Hz, 6H), 1.25–1.50 (m, 24H), 1.80 (quint., J=6.9 Hz, 4H), 3.98 (t, J=6.5 Hz, 4H), 6.94 (d, J=8.9 Hz, 4H), 7.27 (d, J=8.9 Hz, 4H), 7.98 (s, 4H), 8.54 (s, 2H); ^{13}C NMR δ 14.0, 22.7, 26.1, 29.25, 29.36, 29.42, 29.54, 31.9, 68.5, 115.2, 122.3, 128.9, 138.8, 144.6, 157.1, 158.3; MS, *m*/*z* 568 (M^+, 100). Anal. Calcd for $C_{38}H_{52}N_2O_2$: C, 80.24; H, 9.21; N, 4.92. Found: C, 80.16; H, 9.38; N, 4.85.

4.3.7. 1,4-Bis(4-decyloxyphenylimiomethyl)benzene, 1B[10]. Yield 79%; light yellow leaflets (AcOEt): ^{1}H NMR δ 0.89 (t, J=6.8 Hz, 6H), 1.20–1.50 (m, 28H), 1.79 (quint., J=7.0 Hz, 4H), 3.98 (t, J=6.6 Hz, 4H), 6.92 (d, J=8.9 Hz, 4H), 7.24 (d, J=8.6 Hz, 4H), 7.96 (s, 4H), 8.52 (s, 2H); ^{13}C NMR δ 14.0, 22.7, 26.1, 29.3, 29.40, 29.42, 29.57, 29.59, 31.9, 68.5, 115.3, 122.3, 128.9, 138.9, 144.7, 157.1, 158.4; MS, *m*/*z* 596 (M^+, 100). Anal. Calcd for $C_{40}H_{56}N_2O_2$: C, 80.49; H, 9.46; N, 4.69. Found: C, 80.56; H, 9.47; N, 4.60.

4.4. *1,12-Dicarba-closo-dodecaborane-1,12-dicarboxaldehyde, 3A[27]*

Dess–Martin periodinane [8] (6.4 g, 15.1 mmol) was added slowly to a stirred solution of 1,12-bishydroxymethyl-*p*-carborane (**4A**, 1.283 g, 6.29 mmol) in dry CH_3CN (30 ml). The reaction mixture was stirred at r.t. for 2 h and was filtrated through a Celite pad. The filtrate was concentrated and the residue purified by

silica gel column chromatography using AcOEt as the eluant to give 1.099 g (87% yield) of dialdehyde as a colourless solid. ^{1}H NMR δ 1.50–3.75 (brm, 10H), 8.80 (s, 2H). ^{13}C NMR δ 84.4, 184.9; MS, *m/z* 200 (M^+, 100%). HRMS: calcd for $C_4H_{12}B_{10}O_2$ 200.1841; found 200.1826.

4.5. *1,12-Bishydroxymethyl-1,12-dicarba*-closo-*dodecaborane, 4A[9]*

A 1.57M solution of *n*-BuLi (19.46 ml, 30.56 mmol) in *n*-hexane was added dropwise to a stirred solution of *p*-carborane (2.00 g, 13.89 mmol) in anhydrous THF (20 ml) at 0°C under Ar, and the reaction mixture was stirred at r.t. for 30 min. Solid paraformaldehyde $(CH_2O)_n$ (965 mg, 30.56 mmol) was added, the reaction mixture was stirred for 24 h, and poured into water. The resulting mixture was extracted with AcOEt, the organic layer was washed with brine, dried ($MgSO_4$) and concentrated. The crude product was purified by silica gel column chromatography using a hexane/AcOEt mixture (10/1) as the eluant to give 1.459 g (52% yield) of a colourless solid of the diol. ^{1}H NMR (DMSO-d_6) δ 1.50–3.75 (brm, 10H), 1.61 (t, J=7.0 Hz, 2H), 3.50 (t, J=7.3 Hz, 4H). ^{13}C NMR (DMSO-d_6) δ 64.4, 82.1. MS, *m/z* 204 (M^+), 186 (100%). HRMS: calcd for $C_4H_{16}B_{10}O_2$ 204.2154; found 204.2126.

Acknowledgement

This project was supported in part by NSF grant DMR-0111657 and by Grant-in-Aid for Scientific Research (B) No. 13470468, from the Ministry of Education, Culture, Sports, Science and Technology, Japan

References

[1] K. Ohta, A. Januszko, P. Kaszynski, T. Nagamine, G. Sasnouski, Y. Endo. *Liq. Cryst.*, **31**, 671 (2004).
[2] A. Januszko, P. Kaszynski, M.D. Wand, K.M. More, S. Pakhomov, M. O'Neill. *J. mater. Chem.*, **14**, 1544 (2004).
[3] W. Piecek, J.M. Kaufman, P. Kaszynski. *Liq. Cryst.*, **30**, 39 (2003).
[4] P. Kaszynski, A.G. Douglass. *J. organomet. Chem.*, **581**, 28 (1999).
[5] B. Ringstrand, J. Vroman, D. Jensen, A. Januszko, P. Kaszynski, J. Dziaduszek, W. Drzewinski. *Liq. Cryst.* 2005 (ms. 129152).
[6] A. Januszko, P. Kaszynski, K. Ohta, T. Nagamine, V.G., Jr. Young, P. Potaczek, Y. Endo (In prepration).
[7] T. Nagamine, A. Januszko, K. Ohta, P. Kaszynski, Y. Endo (In prepration).
[8] D.B. Dess, J.C. Martin. *J. Am. chem. Soc.*, **113**, 7277 (1991).
[9] V.I. Stanko, Y.V. Goltyapin. *Russ. J. gen. Chem.*, **41**, 2053 (1971).
[10] I. Dierking. *Textures of Liquid Crystals*. Wiley-VCH Weinheim (2003).
[11] G.W. Gray, J.W.G. Goodby. *Smectic Liquid Crystals - Textures and Structures*. Leonard Hill (1984).
[12] S.L. Arora, J.L. Fergason. *Faraday Symp. chem. Soc.*, 97 (1971).
[13] C. Wiegand. *Z. Naturforsch.*, **12b**, 512 (1957).
[14] J.A. Nash, G.W. Gray. *Mol. Cryst. liq. Cryst.*, **25**, 299 (1974).
[15] S.M. Aharoni. *J. polym. Sci. B*, **19**, 281 (1981).
[16] P. Kaszynski (Unpublished results).
[17] Quantum-mechanical calculations were carried out using the Gaussian 98 suite of programs. Geometry optimizations were undertaken at the B3LYP/6-31G(d) and MP2/6-31G(d) levels of theory using C_s symmetry constraints and tight convergence limits. The rotational transition states were located using the QST2 keyword. Thermodynamic correction parameters were obtained at the B3LYP/6-31G(d). Zero-point energy (ZPE) corrections were scaled by 0.9806. M.J. Frisch, G.W. Trucks, H.B. Schlegel, G.E. Scuseria, M.A. Robb, J.R. Cheeseman, V.G. Zakrzewski, J.A. Jr. Montgomery, R.E. Stratmann, J.C. Burant, S. Dapprich, J.M. Millam, A.D. Daniels, K.N. Kudin, M.C. Strain, O. Farkas, J. Tomasi, V. Barone, M. Cossi, R. Cammi, B. Mennucci, C. Pomelli, C. Adamo, S. Clifford, J. Ochterski, G.A. Petersson, P.Y. Ayala, Q. Cui, K. Morokuma, D.K. Malick, A.D. Rabuck, K. Raghavachari, J.B. Foresman, J. Cioslowski, J.V. Ortiz, A.G. Baboul, B.B. Stefanov, G. Liu, A. Liashenko, P. Piskorz, I. Komaromi, R. Gomperts, R.L. Martin, D.J. Fox, T. Keith, M.A. Al-Laham, C.Y. Peng, A. Nanayakkara, C. Gonzalez, M. Challacombe, P.M.W. Gill, B. Johnson, W. Chen, M.W. Wong, J.L. Andres, C. Gonzalez, M. Head-Gordon, E.S. Replogle, J.A. Pople. *Gaussian 98, Revision A. 7*. Gaussian Inc., Pittsburgh PA (1998).
[18] Computational results for PhCHO are in agreement with experimental values of $\Delta G^{\ddagger}$=7.6 kcal mol^{-1} at T=−105°C, see T. Drakenberg, R. Jost, J. Sommer. *Chem. Commun.*, 1011 (1974); and $\Delta H^{\ddagger}$=7.3 kcal mol^{-1}, see D. M. Doddrel, M. R. Bendall, P. F. Barron, D. T. Pegg, *Chem. Commun.*, 77 (1979).
[19] A. Wiegeleben, L. Richter, J. Deresch, D. Demus. *Mol. Cryst. liq. Cryst.*, **59**, 329 (1980).
[20] K. Ohta, A. Januszko, T. Nagamine, R.W. Tilford, P. Kaszynski, Y. Endo (In preparation).
[21] J. Rault, L. Liébert, L. Strzelecki. *Bull. Chim. Soc. Fr.*, 1175 (1975).
[22] The structure of **1B[3]** reported by K. Kishikawa, N. Muramatsu, S. Kohmoto, K. Yamaguchi, M. Yamamoto. *Chem. Mater.*, **15**, 3443 (2003), must have been used mistakenly for another compound.
[23] F. Muzalewski, R. Gawinecki. *Pol. J. Chem.*, **55**, 565 (1981).
[24] D.J. Byron, D.A. Keating, M.T. O'Neill, R.C. Wilson, J.W. Goodby, G.W. Gray. *Mol. Cryst. liq. Cryst.*, **58**, 179 (1980).
[25] D.J. Byron, A.S. Matharu, M. Rees, R.C. Wilson. *Mol. Cryst. liq. Cryst. Sci. Technol. Sect. A*, **258**, 229 (1995).
[26] C.N. Carrigan, R.D. Bartlett, C.S. Esslinger, K.A. Cybulski, P. Tongcharoensirikul, R.J. Bridges, C.M. Thompson. *J. med. Chem.*, **45**, 2260 (2002).
[27] L.I. Zakharkin, V.N. Kalinin. *Synth. React. inorg. met.-org. Chem.*, **2**, 113 (1972).